

Hypothesis Testing in Speckled Data with Stochastic Distances

Abraão D. C. Nascimento, Renato J. Cintra and Alejandro C. Frery, *Member, IEEE*

Abstract—Images obtained with coherent illumination, as is the case of sonar, ultrasound-B, laser and Synthetic Aperture Radar – SAR, are affected by speckle noise which reduces the ability to extract information from the data. Specialized techniques are required to deal with such imagery, which has been modeled by the \mathcal{G}^0 distribution and under which regions with different degrees of roughness and mean brightness can be characterized by two parameters; a third parameter, the number of looks, is related to the overall signal-to-noise ratio. Assessing distances between samples is an important step in image analysis; they provide grounds of the separability and, therefore, of the performance of classification procedures. This work derives and compares eight stochastic distances and assesses the performance of hypothesis tests that employ them and maximum likelihood estimation. We conclude that tests based on the triangular distance have the closest empirical size to the theoretical one, while those based on the arithmetic-geometric distances have the best power. Since the power of tests based on the triangular distance is close to optimum, we conclude that the safest choice is using this distance for hypothesis testing, even when compared with classical distances as Kullback-Leibler and Bhattacharyya.

Index Terms—image analysis, information theory, SAR imagery, speckle noise, multiplicative model, contrast measures.

I. INTRODUCTION

SONAR, laser, Synthetic Aperture Radar (SAR) and ultrasound B-scanners are examples of sensing devices that employ coherent illumination for imaging purposes. In general terms, the operation of these systems consists of sending electromagnetic pulses towards a target and analyzing the returning echo. In particular, the intensity of the echoed signal plays an important role, since it depends on the physical properties of the target surface [1]. Therefore, an accurate modelling of the echo intensity, as well as its associated noise, is determinant to set the extent of the imaging capabilities of a given sensing system.

Noise is inherent to image acquisition. An important source of noise when coherent illumination is used is due to the interference of the signal backscattering by the elements of the target surface. As a consequence of such interference, the returning signal becomes contaminated with fluctuations on its detected intensity. These alterations can significantly

degrade the perceived image quality, as much as the ability of extracting information from the echo data. The resulting effect is called speckled noise [1].

Modelling the probability distribution of image regions can be a venue for image analysis [2]. In particular, the widely employed multiplicative model leads to the suggestion of the \mathcal{G}^0 distribution for data obtained from coherent illumination systems [3]–[7].

A direct statistical approach leads to the use of estimated parameters for data analysis, but a single scalar measure would be more useful when dealing with images. Such measure can be referred to as “contrast” if it provides means for discriminating different types of targets [4], [5], [8]. Suitable measures of contrast not only provide useful information about the image scene but also take part of pre-processing steps in several image analysis procedures [9].

The derivation of expressive contrast measures is important for image understanding. This can be easily done when dealing with optical information, since contrast mainly depends on brightness. In the speckled data case, the main image feature is the roughness. Therefore, contrast measure should take it in account. Nonparametric methods and basic exponential modelling could not include roughness into their framework [10]. Indeed, simple contrast measures, such as the square ratio of the sample mean difference to the sum of the sample variances [4], [5], can offer low computational cost. But, on the other hand, these simple measures can neither provide insight about the roughness nor offer any known statistical property that could furnish hypothesis testing procedures.

Recent years have seen an increasing interest in adapting information-theoretic tools to image processing [8]. In particular, the concept of stochastic divergence [11] has found applications in areas as diverse as image classification [12], cluster analysis [13], and multinomial goodness-of-fit tests [14]. Coherent polarimetric image processing has also benefited, since divergence measures can furnish methods for assessing segmentation algorithms [9]. In [15], the Bhattacharyya distance was proposed as a means to furnish a scalar contrast measure for polarimetric and interferometric SAR imagery.

The aim of this study is to advance the analysis of contrast identification in single channel speckled data. To accomplish this goal, measures of contrast for \mathcal{G}^0 distributed data are proposed and assessed. These measures are based on information theoretic divergences, and we identify the one that best separates different types of targets. This paper extends the results presented in [16], where an exploratory analysis of these distances is presented.

The article unfolds as follows. Section II presents the main

A. D. C. Nascimento is with the Departamento de Estatística, Universidade Federal de Pernambuco, Cidade Universitária, 50740-540, Recife, PE, Brazil, e-mail: abraao.susej@gmail.com

R. J. Cintra is with the Departamento de Estatística, Universidade Federal de Pernambuco, Cidade Universitária, 50740-540, Recife, PE, Brazil, and with the Department of Electrical and Computer Engineering, University of Calgary, Calgary, AB, T2N 1N4, Canada, e-mail: rjds@de.ufpe.br

A. C. Frery is with the Instituto de Computação, Universidade Federal de Alagoas, BR 104 Norte km 97, 57072-970, Maceió, AL, Brazil, email: acfrery@pq.cnpq.br

properties of the model. Section III derives eight contrast measures and discusses their relationships. Section IV presents the main results, namely, the performance of these measures as features for target identification. Conclusions and future lines of research are presented in Section V. Appendix A provides details about the distances derived for the \mathcal{G}^0 model.

II. THE \mathcal{G}^0 DISTRIBUTION FOR SPECKLED DATA

Unlike many classes of noise found in optical imaging, speckled noise is neither Gaussian nor additive [1]. Proposed in the context of optical statistics, the most successful approach for speckle data analysis is the multiplicative model, which emerges from the physics of the image formation [17]. In particular, this model has proven to be accurate for assessing the distribution of the SAR return signal [1].

Such model assumes that each picture element is the outcome of a random variable Z called *return*, which is the product of two independent random variables, X and Y . While the random variable X models the terrain *backscatter*, the random variable Y models the *speckle noise*.

Coherent imaging is able to provide complex-valued information in each pixel [18], but the amplitude or the intensity of such return is the most common format in applications. Without any loss of generality, in this work, only the intensity format for images is examined.

Backscatter carries all the relevant information from the mapped area; it depends on target physical properties as, for instance, moisture and relief. A suitable distribution for the backscatter is the *reciprocal gamma* law [3], $X \sim \Gamma^{-1}(\alpha, \gamma)$, whose density function is given by

$$f_X(x; \alpha, \gamma) = \frac{\gamma^{-\alpha}}{\Gamma(-\alpha)} x^{\alpha-1} \exp\left(-\frac{\gamma}{x}\right), \quad -\alpha, \gamma, x > 0. \quad (1)$$

This parametrization is a particular case of the generalized inverse Gaussian distribution.

Speckle Y is exponentially distributed with unitary mean in single-look intensity images [19]; therefore a multi-look procedure over L independent observations furnishes intensity speckle that can be described by the gamma distribution, $Y \sim \Gamma(L, L)$, with density given by

$$f_Y(y; L) = \frac{L^L}{\Gamma(L)} y^{L-1} \exp(-Ly), \quad y > 0, L \geq 1. \quad (2)$$

In this work, the number of looks L is assumed known and constant over the whole image. A detailed account of the until recently largely unexplored issue of estimating L is provided in [20].

Considering the distributions characterized by densities (1) and (2), and that the related random variables are independent, the distribution associated to $Z = XY$ can be derived and its density is given by

$$f_Z(z; \alpha, \gamma, L) = \frac{L^L \Gamma(L - \alpha)}{\gamma^\alpha \Gamma(-\alpha) \Gamma(L)} z^{L-1} (\gamma + Lz)^{\alpha-L}, \quad -\alpha, \gamma, z > 0, L \geq 1. \quad (3)$$

We indicate this situation as $Z \sim \mathcal{G}^0(\alpha, \gamma, L)$. As shown in [6], this distribution can be used as an universal model for speckled data. Since it has the gamma law as a particular case,

homogeneous targets can be well described [3]. This model can also characterize extremely heterogeneous areas which are left unexplained by the K distribution [18], for instance. Moreover, it is as effective as the K law for modelling heterogeneous data. A multivariate version of this distribution is presented in [18], and its application to image classification is discussed in [21].

The r th moment of Z is expressed by

$$E[Z^r] = \left(\frac{\gamma}{L}\right)^r \frac{\Gamma(-\alpha - r) \Gamma(L + r)}{\Gamma(-\alpha) \Gamma(L)}, \quad (4)$$

if $-r > \alpha$ and infinite otherwise.

Several methods for estimating parameters α and γ are available, including bias-reduced procedures [22]–[24], robust techniques [25], [26] and algorithms for small samples [27]. In this study, because of its optimal asymptotic properties [28], maximum likelihood (ML) estimation is employed to estimate α and γ .

Based on a random sample of size n , $\mathbf{z} = (z_1, z_2, \dots, z_n)$, the likelihood function related to the $\mathcal{G}^0(\alpha, \gamma, L)$ distribution is given by

$$\mathcal{L}(\alpha, \gamma; \mathbf{z}) = \left(\frac{L^L \Gamma(L - \alpha)}{\gamma^\alpha \Gamma(-\alpha) \Gamma(L)}\right)^n \prod_{i=1}^n z_i^{L-1} (\gamma + Lz_i)^{\alpha-L}.$$

Thus, the estimators for α and γ , namely $\hat{\alpha}$ and $\hat{\gamma}$, respectively, are the solution of the following system of non-linear equations:

$$\begin{cases} \psi^0(L - \hat{\alpha}) - \psi^0(-\hat{\alpha}) - \log(\hat{\gamma}) + \frac{1}{n} \sum_{i=1}^n \log(\hat{\gamma} + Lz_i) = 0, \\ -\frac{\hat{\alpha}}{\hat{\gamma}} + \frac{\hat{\alpha} - L}{n} \sum_{i=1}^n (\hat{\gamma} + Lz_i)^{-1} = 0, \end{cases} \quad (5)$$

where $\psi^0(\cdot)$ is the digamma function. However, the above system of equations does not, in general, possess a closed form solution, and numerical optimization methods are considered. We use the BFGS procedure, which is reportedly fast and accurate [29], available in many platforms as, for instance Ox and R .

Figure 1 presents a SAR image obtained by the E-SAR sensor over surroundings of München, Germany [30]; its number of looks was estimated as 3.2. The area exhibits three distinct types of target roughness: (i) homogeneous (corresponding to pasture), (ii) heterogeneous (forest), and (iii) extremely heterogeneous (urban areas). Samples were selected and submitted to statistical analysis. Table I shows the estimates in each of these samples, as well as their size; the last column, namely the number of parts, will be explained later. Figures 2(a), (b), and (c) compare relative frequencies of samples to their associated \mathcal{G}^0 fitted densities for urban, forest, and pasture regions, respectively. The adequacy of the \mathcal{G}^0 law to speckled data is noteworthy. These samples will be used to validate our proposal in section IV-B.

As presented by [7], different SAR image regions can be discriminated using the estimated parameters of the \mathcal{G}^0 model. The expressiveness of the model and the separability of different samples is an open issue that we explore in this work.

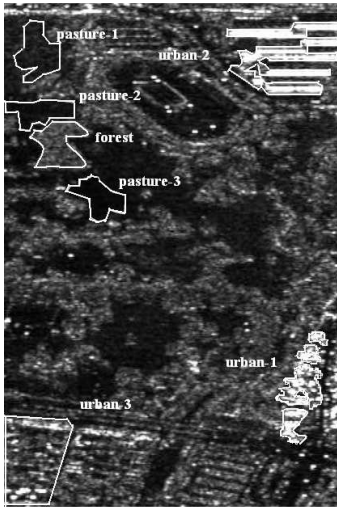


Fig. 1. E-SAR image and selected regions.

TABLE I
PARAMETER ESTIMATES

Regions	$\hat{\alpha}$	$\hat{\gamma}$	$\hat{\mu}$	# pixels	# parts
pasture-1	-15.702	39259	2670.32	1235	25
pasture-2	-12.698	80320	6866.13	1216	24
pasture-3	-11.304	162292	15750.39	1602	32
forest	-9.339	661183	79288.04	1606	32
urban-1	-0.759	148413	∞	2005	40
urban-2	-0.388	110183	∞	3481	71
urban-3	-1.079	55583	703582.30	4657	95

III. MEASURES OF DISTANCE AND CONTRAST UNDER THE \mathcal{G}^0 LAW

Contrast analysis often addresses the problem of quantifying how distinguishable two image regions are from each other. In a sense, the need of a distance is implied. It is possible to understand an image as a set of regions that can be described by different probability laws.

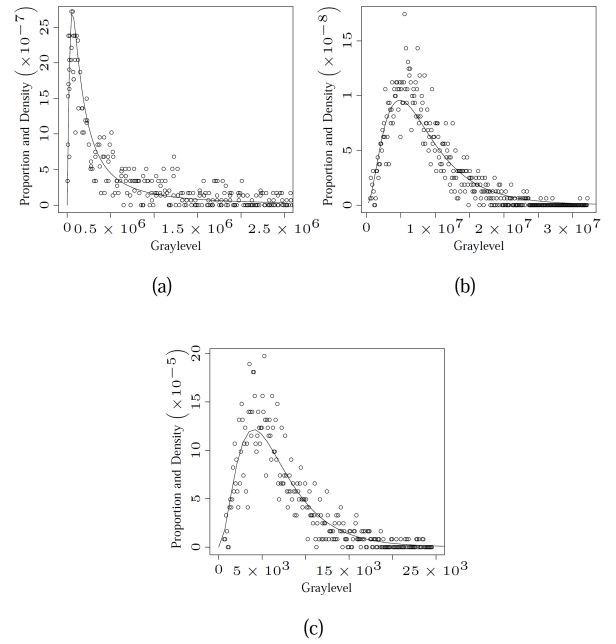
Information theoretical tools collectively known as divergence measures offer entropy based methods to statistically discriminate stochastic distributions [8]. Divergence measures were submitted to a systematic and comprehensive treatment in [31]–[33] and, as a result, the class of (h, ϕ) -divergences was proposed [33].

Let X and Y be random variables defined over the same probability space, equipped with densities $f_X(x; \theta_1)$ and $f_Y(x; \theta_2)$, respectively, where θ_1 and θ_2 are parameter vectors. Assuming that both densities share a common support $I \subset \mathbb{R}$ the (h, ϕ) -divergence, between f_X and f_Y is defined by

$$D_\phi^h(X, Y) = h \left(\int_I \phi \left(\frac{f_X(x; \theta_1)}{f_Y(x; \theta_2)} \right) f_Y(x; \theta_2) dx \right), \quad (6)$$

where $\phi: (0, \infty) \rightarrow [0, \infty)$ is a convex function, $h: (0, \infty) \rightarrow [0, \infty)$ is a strictly increasing function with $h(0) = 0$, and indeterminate forms are assigned value zero.

By a judicious choice of functions h and ϕ , some well-known divergence measures arise. Table II shows the selection of functions h and ϕ that lead with distance measures over which the test powers and sizes were estimated for speckled

Fig. 2. Relative frequencies (\circ) and \mathcal{G}^0 fitted densities (—) for (a) urban, (b) forest, and (c) pasture regions.

data modeled by \mathcal{G}^0 law in [16]. Specifically, the following measures were examined: (i) the Kullback-Leibler divergence [34], (ii) the relative Rényi (also known as Chernoff) divergence of order β [35], [36], (iii) the Hellinger distance [37], (iv) the Bhattacharyya distance [38], (v) the relative Jensen-Shannon divergence [39], (vi) the relative arithmetic-geometric divergence [40], (vii) the triangular distance [41], and (viii) the harmonic-mean distance [41].

Often not rigorously a metric [42], since the triangle inequality does not necessarily holds, divergence measures are mathematically suitable tools in the context of comparing the distribution of random variables [43]. Additionally, some of the divergence measures lack the symmetry property. Although there are numerous methods to address the symmetry problem [44], a simple solution is to define a new measure d_ϕ^h given by

$$d_\phi^h(X, Y) = \frac{D_\phi^h(X, Y) + D_\phi^h(Y, X)}{2}, \quad (7)$$

regardless whether $D_\phi^h(\cdot, \cdot)$ is symmetric or not. Henceforth, the symmetrized versions of the divergence measures are termed “distances”. By applying the functions of Table II into equation (6), and symmetrizing the resulting divergences, integral formulas for the distance measures are obtained. For simplicity, in the list below, we suppress the explicit dependence on x and the support I in the notation.

(i) The Kullback-Leibler distance:

$$d_{\text{KL}}(X, Y) = \frac{1}{2} \int (f_X - f_Y) \log \left(\frac{f_X}{f_Y} \right).$$

(ii) The Rényi distance of order β :

$$d_{\text{R}}^\beta(X, Y) = \frac{1}{\beta - 1} \log \left(\frac{\int f_X^\beta f_Y^{1-\beta} + \int f_X^{1-\beta} f_Y^\beta}{2} \right).$$

TABLE II
 (h, ϕ) -DIVERGENCES AND RELATED FUNCTIONS ϕ AND h

(h, ϕ) -divergence	$h(y)$	$\phi(x)$
Kullback-Leibler	y	$x \log(x)$
Rényi (order β)	$\frac{1}{\beta-1} \log((\beta-1)y+1), 0 \leq y < \frac{1}{1-\beta}$	$\frac{x^\beta - \beta(x-1) - 1}{\beta-1}, 0 < \beta < 1$
Hellinger	$y/2, 0 \leq y < 2$	$(\sqrt{x}-1)^2$
Bhattacharyya	$-\log(-y+1), 0 \leq y < 1$	$-\sqrt{x} + \frac{x+1}{2}$
Jensen-Shannon	y	$x \log\left(\frac{2x}{x+1}\right)$
Arithmetic-geometric	y	$\left(\frac{x+1}{2}\right) \log\left(\frac{x+1}{2x}\right)$
Triangular	$y, 0 \leq y < 2$	$\frac{(x-1)^2}{x+1}$
Harmonic-mean	$-\log\left(-\frac{y}{2}+1\right), 0 \leq y < 2$	$\frac{(x-1)^2}{x+1}$

(iii) The Hellinger distance:

$$d_H(X, Y) = 1 - \int \sqrt{f_X f_Y} = 1 - \exp\left(-\frac{1}{2} d_R^{1/2}(X, Y)\right).$$

(iv) The Bhattacharyya distance:

$$d_B(X, Y) = -\log\left(\int \sqrt{f_X f_Y}\right) = -\log(1 - d_H(X, Y)).$$

(v) The Jensen-Shannon distance:

$$d_{JS}(X, Y) = \frac{1}{2} \left[\int f_X \log\left(\frac{2f_X}{f_Y + f_X}\right) + \int f_Y \log\left(\frac{2f_Y}{f_Y + f_X}\right) \right].$$

(vi) The arithmetic-geometric distance:

$$d_{AG}(X, Y) = \frac{1}{2} \int (f_X + f_Y) \log\left(\frac{f_Y + f_X}{2\sqrt{f_Y f_X}}\right).$$

(vii) The triangular distance:

$$d_T(X, Y) = \int \frac{(f_X - f_Y)^2}{f_X + f_Y}.$$

(viii) The harmonic-mean distance:

$$\begin{aligned} d_{HM}(X, Y) &= -\log\left(\int \frac{2f_X f_Y}{f_X + f_Y}\right) \\ &= -\log\left(1 - \frac{d_T(X, Y)}{2}\right). \end{aligned}$$

Alternatively, the distances can be put under the (h, ϕ) -formalism. The distances derived from symmetric divergences inherit the same h and ϕ functions. For the remaining distances, specifically tailored h and ϕ functions can be found as shown in Table III.

Provided that the concerned random variables follow the \mathcal{G}^0 law with parameter vectors $\theta_1 = (\alpha_1, \gamma_1, L_1)$ and $\theta_2 = (\alpha_2, \gamma_2, L_2)$, particular expressions for the discussed distances can be achieved. After adequate considerations, the integral forms of some of the distances furnish closed expressions. Appendix A details the mathematical manipulations employed to derive the Kullback-Leibler, Rényi of order β , Hellinger, and Bhattacharyya distances between two \mathcal{G}^0 distributed random variables. By contrast, no corresponding closed form expressions were found for the triangular, Jensen-Shannon, arithmetic-geometric, and harmonic-mean distances. In order to evaluate them, numerically quadrature routines available for the `Ox` programming language were employed [45].

When considering the distance between same distributions, only their parameters are relevant. In this case, parameter vectors θ_1 and θ_2 replace random variables symbols X and Y as the arguments of divergence and distance measures. This notation is in agreement with that of [33].

Figure 3 depicts plots for the distances $d_\phi^h(\theta_1, \theta_2)$ between \mathcal{G}^0 , where $\theta_1 = (\alpha_1, \gamma_1, 8)$ and $\theta_2 = (-12, 11, 8)$. Parameter α_1 ranges in the interval $[-14, -10]$ and γ_1 was selected, using equation (4), so that its associated \mathcal{G}^0 distributed random variable has unit mean:

$$\gamma_1 = \frac{L\Gamma(-\alpha_1)\Gamma(L)}{\Gamma(-\alpha_1 - 1)\Gamma(L + 1)} = -\alpha_1 - 1. \quad (8)$$

The obtained curves indicate that Hellinger and Bhattacharyya distances exhibit comparable behavior. Similarly, Kullback-Leibler, Rényi with $\beta = 0.95$, and triangular distances have closely matching plots.

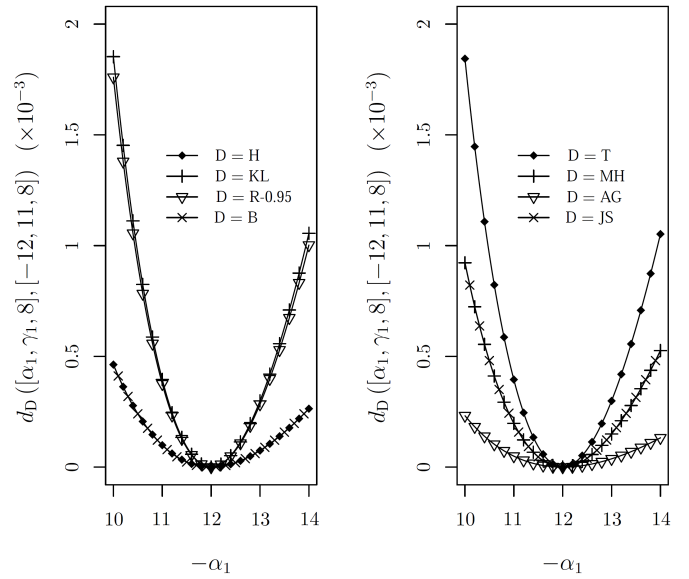


Fig. 3. Distance measures between two \mathcal{G}^0 distributed random variables as a function of α_1 .

Several convergence properties of the (h, ϕ) -divergences were established in [33]. Under the regularity conditions discussed in [33, p.380], if parameter vectors θ_1 and θ_2 are

TABLE III
(h, ϕ)-DISTANCES AND THEIR FUNCTIONS ϕ AND h

(h, ϕ)-distance	$h(y)$	$\phi(x)$
Kullback-Leibler	$y/2$	$(x-1) \log(x)$
Rényi (order β)	$\frac{1}{\beta-1} \log((\beta-1)y+1), 0 \leq y < \frac{1}{1-\beta}$	$\frac{x^{1-\beta} + x^{\beta} - \beta(x-1) - 2}{2(\beta-1)}, 0 < \beta < 1$
Jensen-Shannon	$y/2$	$x \log\left(\frac{2x}{x+1}\right) + \log\left(\frac{2}{x+1}\right)$
Arithmetic-geometric	y	$\left(\frac{x+1}{2}\right) \log\left(\frac{x+1}{2x}\right) + \left(\frac{x-1}{2}\right)$

equal, then, as $m, n \rightarrow \infty$, the quantity

$$\frac{2mn}{m+n} \frac{D_{\phi}^h(\widehat{\boldsymbol{\theta}}_1, \widehat{\boldsymbol{\theta}}_2)}{h'(0)\phi''(1)}$$

is asymptotically chi-square distributed with M degrees of freedom, where $\widehat{\boldsymbol{\theta}}_1 = (\widehat{\theta}_{11}, \dots, \widehat{\theta}_{1M})$ and $\widehat{\boldsymbol{\theta}}_2 = (\widehat{\theta}_{21}, \dots, \widehat{\theta}_{2M})$ are the ML estimators of $\boldsymbol{\theta}_1$ and $\boldsymbol{\theta}_2$ based on independent samples of sizes m and n , respectively [33].

Thus, when considering the definition of the distances in terms of the h and ϕ functions, and applying the results on the convergence in distribution of the (h, ϕ)-measures to χ_M^2 [33], the lemma asserted below is proved.

Lemma 1: Let the regularity conditions proposed in [33, p.380] hold. If $\frac{m}{m+n} \xrightarrow{m, n \rightarrow \infty} \lambda \in (0, 1)$ and $\boldsymbol{\theta}_1 = \boldsymbol{\theta}_2$, then

$$\frac{2mn}{m+n} \frac{d_{\phi}^h(\widehat{\boldsymbol{\theta}}_1, \widehat{\boldsymbol{\theta}}_2)}{h'(0)\phi''(1)} \xrightarrow{m, n \rightarrow \infty} \mathcal{D} \chi_M^2, \quad (9)$$

where “ \mathcal{D} ” denotes convergence in distribution.

Based on Lemma 1, statistical hypothesis tests for the null hypothesis $\boldsymbol{\theta}_1 = \boldsymbol{\theta}_2$ can be derived. In particular, the following statistic is considered:

$$S_{\phi}^h(\widehat{\boldsymbol{\theta}}_1, \widehat{\boldsymbol{\theta}}_2) = \frac{2mnv}{m+n} d_{\phi}^h(\widehat{\boldsymbol{\theta}}_1, \widehat{\boldsymbol{\theta}}_2),$$

where $v = 1/(h'(0)\phi''(1))$ is a constant that depends on the chosen distance. Table IV lists the values of v for each examined distance. We are now in position to state the following result.

Proposition 1: Let m and n assume large values and $S_{\phi}^h(\widehat{\boldsymbol{\theta}}_1, \widehat{\boldsymbol{\theta}}_2) = s$, then the null hypothesis $\boldsymbol{\theta}_1 = \boldsymbol{\theta}_2$ can be rejected at a level η if $\Pr(\chi_M^2 > s) \leq \eta$.

In terms of image analysis, this proposition offers a method to statistically refute the hypothesis that two samples obtained in different regions can be described by the same distribution.

TABLE IV
DISTANCES AND CONSTANTS v

Distance	v
Kullback-Leibler	1
Rényi (order β)	$1/\beta$
Hellinger	4
Bhattacharyya	4
Jensen-Shannon	4
Arithmetic-geometric	4
Triangular	1
Harmonic-mean	2

IV. RESULTS AND DISCUSSION

In order to assess the proposed contrast measures, both synthetic \mathcal{G}^0 distributed data and actual SAR images were submitted to the statistical analysis suggested by Proposition 1. Two nominal levels of significance were considered, namely 1% and 5%. These results are presented in sections IV-A and IV-B, respectively.

Usually SAR images are analyzed in square arrays of size 7×7 , 9×9 , and 11×11 pixels. In a conservative way, we chose to work with the smallest sample size, i.e., windows of size 7×7 pixels, but we present a summary of results for larger windows, i.e., 9×9 and 11×11 .

A. Analysis with Simulated Data

Although the \mathcal{G}^0 distribution is specified by α and γ , SAR literature often employs the texture α and the mean μ . Since equation (4) establishes that

$$\mu = \frac{\gamma}{L} \frac{\Gamma(-\alpha-1) \Gamma(L+1)}{\Gamma(-\alpha) \Gamma(L)} = -\frac{\gamma}{1+\alpha},$$

both specifications are equivalent. Thus, prescribing the parameter values of $\alpha \in \{-1.5, -3, -5, -8\}$, $\mu \in \{1, 2, 5, 10\}$, and $L \in \{1, 2, 4, 8\}$, a total of 64 statistically different image types will be used in the following assessment.

The empirical size and power of the proposed test were sought as a means to guide the identification of the most adequate distance measure. To obtain the pursued empirical data, Monte Carlo experiments under different scenarios were designed. Let two \mathcal{G}^0 distributed images be specified by the parameter vectors (α_1, μ_1, L) and (α_2, μ_2, L) , for $L \in \{1, 2, 4, 8\}$. Four scenarios were considered in such a way that image pairs under scrutiny satisfy: (i) $\alpha_1 = \alpha_2, \mu_1 \neq \mu_2$, (ii) $\alpha_1 \neq \alpha_2, \mu_1 = \mu_2$, (iii) $\alpha_1 < \alpha_2, \mu_1 < \mu_2$, or (iv) $\alpha_1 < \alpha_2, \mu_1 > \mu_2$.

Situation (i) corresponds to $\gamma_1 \neq \gamma_2$ and $\alpha_1 = \alpha_2$. For the other three situations, let $\kappa = (1+\alpha_1)/(1+\alpha_2)$. Situation (ii) is $\gamma_1 = \kappa\gamma_2$ and $\alpha_1 \neq \alpha_2$. Situation (iii) is $\gamma_1/\gamma_2 > \kappa$ and $\alpha_1 < \alpha_2$. Finally, situation (iv) is $\gamma_1/\gamma_2 < \kappa$ and $\alpha_1 < \alpha_2$. For the given selection of parameter values, pairwise combinations of the 64 image types furnished 96 different cases for each scenario (i) or (ii). Situations (iii) and (iv) offered 144 cases each.

Situation (i) describes a tough task: discriminating two targets with equal mean brightness that only differ on the roughness. Situation (ii) models the situation where areas with equal roughness have different mean brightness. Situations (iii) and (iv) describe pairs of targets whose roughness and mean brightness are both different, but with different relations.

Images submitted to the suggested statistical test for homogeneity must have their distribution parameters estimated. However, the employed ML estimators for \mathcal{G}^0 distributed data are often difficult to be evaluated due to numerical instability issues [24]. This problem was previously reported in [27], and estimate censoring was proposed as a procedure to circumvent this situation. Given a sample, we compute the ML estimators $(\hat{\alpha}, \hat{\gamma})$ defined in equation set (5) and apply censoring as explained below.

Monte Carlo simulations were performed for each scenario and only those results where $\hat{\alpha} \in [10\alpha, \alpha/20]$ were recorded valid. Up to 5500 replications were considered and, as presented in the following tables in the ‘Rep’ column, at least 1343 valid replications were obtained. All computations were performed using the Ox programming language [29]; in particular, the quasi-Newton method with analytical derivatives was used to obtain the estimates.

In the following, we report the null rejection rates of tests whose statistics S_{ϕ}^h are based on the discussed stochastic distances: Kullback-Leibler (S_{KL}), Rényi of order $\beta = 0.95$ (S_R), Hellinger (S_H), Bhattacharyya (S_B), Jensen-Shannon (S_{JS}), arithmetic-geometric (S_{AG}), triangular (S_T), and harmonic-mean (S_{HM}). Data was simulated obeying the null hypothesis $\mathcal{H}_0 : (\alpha_1, \gamma_1) = (\alpha_2, \gamma_2) = (\alpha^*, \gamma^*)$.

Table V presents the empirical sizes (rejection rates of samples from the same distribution) of the tests at nominal levels 1% and 5%. The changes in the value of γ^* for a specific L do not alter significantly the rate of type I error. Although changes of scale do not alter the distance between distributions, the application of the maximum likelihood estimation could raise concerns. Such estimation method is known (i) to be prone to severe numerical instabilities and (ii) to increase the estimator variance when α is reduced. In spite of these facts, the test performance was little affected.

For smaller values of α^* (homogeneous images), the empirical sizes are reduced; this is due to the fact that the \mathcal{G}^0 distribution becomes progressively insensitive to changes of α , i.e., the relative difference between densities is more pronounced for the same variation of α when this texture parameter is larger. The triangular distance presents the optimum performance regarding test size, since its Type I error is closest to the nominal values. The tests yielded the empirical size closest to the theoretical one as follows: triangular and harmonic-mean in all of the 64 situations, Jensen-Shannon in 98.44%, Hellinger in 90.63%, Bhattacharyya in 85.94%, Rényi in 75%, Kullback-Leibler in 73.44%, and, finally, arithmetic-geometric in 56.25%. The lowest of these cases are highlighted in boldface type in Table V. It is noteworthy that the two most commonly employed distances, namely the Kullback-Leibler and the Bhattacharyya distances, presented poor performances when used as test statistics.

The efficiency of the measures S_T , S_B , S_R , S_H , and S_{JS} with regard to S_{KL} is another important fact, since it is common to use measures based in the Kullback-Leibler classic divergence.

Tables VI, VII, VIII, and IX complete the analysis of the tests based on stochastic distances by presenting their empirical power, i.e., the rejection rates when samples from different distributions are contrasted.

Table VI presents the empirical power of the tests at 1% and 5% nominal levels when $\alpha_1 = \alpha_2$ and $\mu_1 \neq \mu_2$. This situation evaluates the effect of the change of mean gray level while keeping the roughness constant. For fixed L , the test power increases as the ratio γ_2/γ_1 increases. Additionally, increasing the number of looks enhances the power of the test. The power is larger for smaller values of α , i.e., in homogeneous targets, which is in agreement with the aforementioned sensitivity of the distribution to the texture parameter. In general, the empirical power is high. For example, it is greater than 61.89% for $L \geq 4$.

In summary, these tests are able to recognize images of same roughness with different mean brightness. The arithmetic-geometric distance provides the best test for small values of L (highlighted in boldface type in Table VI when there are no matching situations).

It is noteworthy that as L increases there is a threshold for which all tests exhibit the same performance. The more homogeneous the target, the smaller this threshold is. As expected, it is easier to perform sound statistical tests on homogeneous areas than in heterogeneous or extremely heterogeneous targets. More looks are needed in the latter cases for attaining the same power.

Table VII presents the empirical power of tests at 1% and 5% nominal levels for the case of equal mean brightness ($\mu_1 = \mu_2$) but different roughness ($\alpha_1 \neq \alpha_2$). The test based on the arithmetic-geometric distance consistently has the best performance regarding this criterion, with a few situations where other tests match it.

As previously said, the task of discriminating targets of same mean brightness, but different roughness is tough. There are situations where the power of the best test is as low as 0.71 (when $\alpha_1 = -5$, $\alpha_2 = -8$, $\gamma_1 = 8$, $\gamma_2 = 14$ and $L = 1$) but, for fixed $\alpha_1 \neq \alpha_2$ the power increases with the rate γ_1/γ_2 and with the number of looks. The former situation is illustrated in Figure 4.

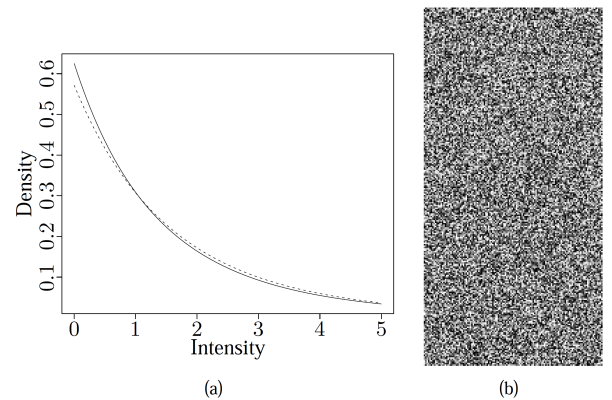


Fig. 4. A tough problem: (a) densities of the $\mathcal{G}^0(-5, 8, 1)$ and $\mathcal{G}^0(-8, 14, 1)$ distributions (solid and dashes, respectively) and (b) the associated data (upper and lower half, resp.)

The worst cases, i.e., those with smallest power, are related to small values of α which correspond to homogeneous areas. The distance between \mathcal{G}^0 distributions becomes less sensitive to different roughness in such targets.

TABLE V
REJECTION RATES OF (h, ϕ) -DIVERGENCE TESTS UNDER $H_0: (\alpha_1, \gamma_1) = (\alpha_2, \gamma_2) = (\alpha^*, \gamma^*)$, $\alpha^* \in \{-1.5, -3, -5, -8\}$

α^*	γ^*	L	1% nominal level									5% nominal level									Rep
			S_{KL}	S_H	S_T	S_B	S_{JS}	S_{HM}	S_{AG}	S_R	S_{KL}	S_H	S_T	S_B	S_{JS}	S_{HM}	S_{AG}	S_R			
-1.5	0.5	1	1.06	0.65	0.40	0.71	0.52	0.50	1.79	0.98	4.58	3.31	2.21	3.56	2.85	2.54	6.27	4.37	4802		
		2	1.27	0.82	0.52	0.88	0.69	0.60	2.34	1.10	5.97	4.69	3.29	4.96	4.10	3.65	7.44	5.76	5347		
		4	1.39	0.86	0.42	1.00	0.57	0.53	2.14	1.30	6.03	5.28	3.69	5.46	4.60	4.15	7.69	5.81	5473		
		8	1.71	1.16	0.58	1.27	0.87	0.80	2.57	1.67	6.51	5.51	4.04	5.90	4.89	4.46	7.77	6.39	5496		
	5	1	0.71	0.38	0.25	0.46	0.31	0.29	1.38	0.58	4.22	3.05	1.98	3.30	2.63	2.38	5.91	4.01	4792		
		2	1.20	0.81	0.47	0.90	0.60	0.56	1.99	1.11	5.97	4.92	3.15	5.20	4.06	3.57	7.98	5.76	5326		
		4	1.59	1.13	0.55	1.23	0.82	0.75	2.49	1.54	6.35	5.40	3.99	5.63	4.85	4.39	7.75	6.16	5468		
		8	1.60	0.95	0.51	1.11	0.73	0.64	2.47	1.55	6.84	5.82	4.48	6.20	5.22	4.86	8.17	6.77	5497		
-3.0	2	1	0.47	0.34	0.22	0.41	0.31	0.31	0.88	0.47	3.01	2.19	1.47	2.41	1.91	1.82	3.61	2.88	3190		
		2	0.51	0.35	0.16	0.37	0.30	0.23	0.83	0.49	3.21	2.36	1.85	2.52	2.17	1.94	4.23	3.14	4329		
		4	0.92	0.61	0.31	0.70	0.41	0.41	1.39	0.88	4.67	3.97	2.72	4.17	3.56	3.25	5.97	4.56	5113		
		8	1.20	0.81	0.33	0.92	0.57	0.46	1.86	1.09	5.78	4.98	3.41	5.19	4.21	3.78	7.07	5.57	5419		
	20	1	0.54	0.29	0.22	0.35	0.25	0.29	0.80	0.48	2.96	2.45	1.69	2.55	1.97	1.94	3.76	2.77	3140		
		2	0.62	0.49	0.25	0.51	0.39	0.37	0.97	0.55	3.44	2.87	2.40	3.00	2.61	2.52	4.67	3.30	4327		
		4	0.77	0.53	0.31	0.61	0.49	0.43	1.39	0.71	4.96	3.88	2.88	4.12	3.35	3.24	6.34	4.71	5098		
		8	1.27	0.89	0.44	1.01	0.70	0.53	2.07	1.18	5.64	4.69	3.39	4.89	4.17	3.82	6.84	5.52	5421		
-5.0	4	1	0.28	0.23	0.18	0.23	0.18	0.18	0.64	0.28	2.16	1.70	1.56	1.88	1.56	1.56	2.75	2.07	2178		
		2	0.57	0.47	0.31	0.47	0.41	0.41	0.66	0.47	2.64	2.14	1.67	2.23	1.95	1.92	3.12	2.55	3177		
		4	0.64	0.36	0.27	0.48	0.36	0.34	0.84	0.61	2.98	2.46	1.82	2.55	2.23	2.02	4.05	2.89	4398		
		8	1.00	0.75	0.37	0.85	0.63	0.53	1.58	1.00	4.90	3.96	3.15	4.25	3.68	3.47	6.30	4.71	5077		
	40	1	0.33	0.24	0.14	0.33	0.14	0.14	0.57	0.33	2.05	1.62	1.14	1.81	1.38	1.24	2.67	2.00	2098		
		2	0.40	0.34	0.31	0.34	0.34	0.34	0.83	0.34	2.88	2.41	1.89	2.54	2.20	2.10	3.46	2.81	3234		
		4	0.50	0.27	0.16	0.39	0.23	0.23	0.78	0.43	2.95	2.38	1.69	2.51	2.13	1.90	4.23	2.74	4374		
		8	0.96	0.67	0.37	0.77	0.55	0.49	1.39	0.90	4.50	3.79	2.51	4.02	3.32	2.85	5.95	4.38	5094		
-8.0	7	1	0.33	0.26	0.07	0.26	0.26	0.26	0.46	0.33	1.89	1.56	1.30	1.69	1.50	1.30	2.54	1.76	1536		
		2	0.13	0.08	0.08	0.08	0.08	0.08	0.29	0.13	1.75	1.46	0.96	1.50	1.25	1.25	2.05	1.67	2394		
		4	0.32	0.29	0.06	0.32	0.26	0.23	0.47	0.32	1.90	1.69	1.32	1.72	1.61	1.49	2.72	1.87	3422		
		8	0.61	0.42	0.13	0.48	0.24	0.24	0.87	0.59	3.45	2.84	2.12	3.06	2.49	2.38	4.33	3.32	4575		
	70	1	0.08	0.08	0.08	0.08	0.08	0.08	0.23	0.08	1.92	1.77	1.54	1.85	1.69	1.54	2.39	1.85	1299		
		2	0.36	0.31	0.22	0.36	0.27	0.27	0.54	0.36	2.23	1.96	1.52	2.01	1.70	1.70	2.90	2.10	2241		
		4	0.52	0.47	0.17	0.50	0.32	0.35	0.73	0.52	2.77	2.50	2.01	2.68	2.39	2.27	3.44	2.74	3434		
		8	0.66	0.51	0.31	0.53	0.44	0.42	1.00	0.64	3.63	3.15	2.19	3.32	2.77	2.64	4.72	3.55	4512		

Table VIII presents the empirical power of tests at 1% and 5% nominal levels for the case $\alpha_1 > \alpha_2$ and $\mu_1 < \mu_2$. In general, the powers are large in this case but the best test regarding this criterion is the one based on the arithmetic-geometric distance. As expected, the power increases with the number of looks and with the parameter difference.

Table IX presents the empirical powers of test at 1% and 5% nominal levels for the case $\alpha_1 > \alpha_2$ and $\mu_1 > \mu_2$. Considering L fixed, it suggests that the empirical test power is nearly the same for a value of the ratio γ_2/γ_1 . Moreover, these empirical powers increase with the number of looks L .

Table X illustrates the performance of the tests with respect to the sample size. It shows the rejection rates in the same situation which Table VI reports in detail for $N = 49$, i.e., $L = 1$, $\gamma_2/\gamma_1 = 2$ and $\alpha \in \{-1.5, -3, -5, -8\}$. This table shows that when the sample size varies $N \in \{49, 81, 121\}$ the bigger the sample the more powerful all the tests are and, therefore, better discrimination is achieved.

B. SAR Data Analysis

In this section we use the data presented in Figure 1 and analyzed in Table I as a means for validating the simulation results obtained in section IV-A.

Each of the seven labelled regions, i.e, urban-1, -2, -3, forest and pasture-1, -2, -3, was partitioned into disjoint 7×7 pixel samples; the number of samples (parts) is presented in the last column of Table I.

All pairs of parts (both from the same and different regions) were submitted to the proposed statistical tests. Pairs coming from the same region served to compute the Type I errors,

TABLE X
REJECTION RATES OF (h, ϕ) -DIVERGENCE TESTS UNDER $H_1: (\alpha_1, \gamma_1) \neq (\alpha_2, \gamma_2)$ WHERE $\alpha_1 = \alpha_2 \in \{-1.5, -3, -5, -8\}$, $L = 1$, $\gamma_1/\gamma_2 = 2$ AND SAMPLE SIZE N

α	N	1% nominal level				5% nominal level				Rep
		S_{KL}	S_T	S_B	S_{AG}	S_{KL}	S_T	S_B	S_{AG}	
-1.5	49	28.56	22.15	27.68	31.29	50.36	45.59	49.93	52.95	5133
	81	53.24	48.79	52.51	55.52	74.61	72.23	74.44	76.00	5391
	121	75.04	72.68	74.84	75.85	90.15	89.27	89.98	90.59	5461
-3	49	39.34	30.70	37.87	42.63	62.42	57.08	61.31	64.20	4143
	81	68.03	63.52	67.26	70.14	85.30	83.24	84.93	86.26	4679
	121	88.64	86.89	88.42	89.42	96.89	96.29	96.83	97.15	5010
-5	49	44.88	35.28	43.24	49.31	68.28	62.53	66.88	70.44	3427
	81	75.65	70.50	75.01	77.89	91.00	88.70	90.49	91.59	3922
	121	94.30	92.73	93.93	94.58	98.39	98.13	98.36	98.55	4280
-8	49	48.62	38.61	46.83	53.17	72.02	65.40	70.87	74.26	2945
	81	80.10	74.80	78.90	82.15	92.74	90.63	92.31	93.29	3266
	121	96.00	94.77	95.81	96.55	99.21	99.01	99.15	99.45	3651

while pairs extracted from different regions were used to calculate the Type II errors under the hypothesis $\alpha_1 > \alpha_2$ and $\mu_1 > \mu_2$, in accordance with the estimates shown in Table I.

Table XI presents the observed rejections rates of samples from the same region. The results show that all the tests have excellent performance for pasture and forest regions with respect to this criterion. In urban scenarios the results show that S_{KL} , S_T and S_{JS} maintain the good performance. Two additional observation are noteworthy: the S_{AG} test shows optimal size only at the 1% level, and the S_H , S_B , and S_R classical test present an instability in the estimated size, as well as S_{AG} when the nominal level is 5%.

As previously mentioned, the \mathcal{G}^0 distribution is quite sensitive to the roughness parameter in extremely heterogeneous situations, and small random fluctuations may produce test statistics leading to rejection. The test size decreases with the

TABLE XII
REJECTION RATES OF (h, ϕ) -DIVERGENCE TESTS UNDER $H_1: (\alpha_1, \gamma_1) \neq (\alpha_2, \gamma_2)$, WITH $\mu_1 = \mu_2$

Regions	S_{KL}	S_H	S_T	S_B	S_{JS}	S_{HM}	S_{AG}	S_R	S_{KL}	S_H	S_T	S_B	S_{JS}	S_{HM}	S_{AG}	S_R	P
pasture-1×pasture-2	100.00	100.00	100.00	100.00	100.00	100.00	100.00	100.00	100.00	100.00	100.00	100.00	100.00	100.00	100.00	100.00	600
pasture-1×pasture-3	100.00	100.00	100.00	100.00	100.00	100.00	100.00	100.00	100.00	100.00	100.00	100.00	100.00	100.00	100.00	100.00	400
pasture-2×pasture-3	94.64	89.13	87.50	90.48	88.41	88.41	96.38	90.58	98.21	98.21	97.02	98.21	97.02	97.02	98.21	98.21	384
forest×pasture-1	100.00	100.00	100.00	100.00	100.00	100.00	100.00	100.00	100.00	100.00	100.00	100.00	100.00	100.00	100.00	100.00	625
forest×pasture-2	100.00	100.00	100.00	100.00	100.00	100.00	100.00	100.00	100.00	100.00	100.00	100.00	100.00	100.00	100.00	100.00	600
forest×pasture-3	100.00	100.00	100.00	100.00	100.00	100.00	100.00	100.00	100.00	100.00	100.00	100.00	100.00	100.00	100.00	100.00	400
urban-1×pasture-1	100.00	100.00	100.00	100.00	100.00	100.00	100.00	100.00	100.00	100.00	100.00	100.00	100.00	100.00	100.00	100.00	1000
urban-1×pasture-2	100.00	100.00	100.00	100.00	100.00	100.00	100.00	100.00	100.00	100.00	100.00	100.00	100.00	100.00	100.00	100.00	960
urban-1×pasture-3	100.00	100.00	100.00	100.00	100.00	100.00	100.00	100.00	100.00	100.00	100.00	100.00	100.00	100.00	100.00	100.00	640
urban-2×pasture-1	100.00	100.00	100.00	100.00	100.00	100.00	100.00	100.00	100.00	100.00	100.00	100.00	100.00	100.00	100.00	100.00	1775
urban-2×pasture-2	100.00	100.00	100.00	100.00	100.00	100.00	100.00	100.00	100.00	100.00	100.00	100.00	100.00	100.00	100.00	100.00	1704
urban-2×pasture-3	100.00	100.00	100.00	100.00	100.00	100.00	100.00	100.00	100.00	100.00	100.00	100.00	100.00	100.00	100.00	100.00	1136
urban-3×pasture-1	100.00	100.00	100.00	100.00	100.00	100.00	100.00	100.00	100.00	100.00	100.00	100.00	100.00	100.00	100.00	100.00	2375
urban-3×pasture-2	100.00	100.00	100.00	100.00	100.00	100.00	100.00	100.00	100.00	100.00	100.00	100.00	100.00	100.00	100.00	100.00	2280
urban-3×pasture-3	100.00	100.00	100.00	100.00	100.00	100.00	100.00	100.00	100.00	100.00	100.00	100.00	100.00	100.00	100.00	100.00	1520
urban-1×forest	98.70	99.70	98.10	99.70	98.50	99.20	98.40	99.80	98.90	100.00	99.10	100.00	99.50	99.80	100.00	100.00	1000
urban-2×forest	98.03	100.00	99.49	100.00	99.27	100.00	97.30	100.00	98.03	100.00	99.49	100.00	99.27	100.00	100.00	100.00	1775
urban-3×forest	94.74	91.12	80.17	91.79	87.37	86.06	96.17	89.39	97.73	96.97	92.97	97.39	95.54	95.71	95.58	95.58	2375
urban-1×urban-2	29.68	93.98	26.37	94.19	27.75	73.73	30.60	100.00	43.13	98.27	41.48	98.31	42.08	92.89	100.00	100.00	2840
urban-2×urban-3	91.05	93.97	89.92	94.26	90.34	92.32	91.50	96.18	95.05	96.45	94.47	96.55	94.71	95.71	97.84	97.84	6725
urban-1×urban-3	98.84	100.00	98.50	100.00	98.74	100.00	99.01	100.00	99.69	100.00	99.67	100.00	99.70	100.00	100.00	100.00	3800

(i) The Kullback-Leibler distance:

$$d_{KL}(\theta_1, \theta_2) = \sum_{i=1}^2 (-1)^i k_i d \int_0^\infty \frac{x^{a_i}}{(b_i + L_i x)^{c_i}} dx + \sum_{i=1}^2 (-1)^i k_i d \int_0^\infty \frac{\log(b_i + L_i x) x^{a_i}}{(b_i + L_i x)^{c_i}} dx + \sum_{i=1}^2 (-1)^i k_i (L_2 - L_1) \int_0^\infty \frac{\log(x) x^{a_i}}{(b_i + L_i x)^{c_i}} dx - k_1 d \int_0^\infty \frac{x^{a_1} \log(b_2 + L_2 x)}{(b_1 + L_1 x)^{c_1}} dx + k_2 d \int_0^\infty \frac{x^{a_2} \log(b_1 + L_1 x)}{(b_2 + L_2 x)^{c_2}} dx,$$

where $k_i = \frac{L_i^{L_i} \Gamma(L_i - \alpha_i)}{(\frac{L_i}{2})^{\alpha_i} \Gamma(\alpha_i) \Gamma(L_i)}$, $a_i = L_i - 1$, $b_i = \frac{\gamma_i}{2}$, $c_i = |\alpha_i| + L_i$ for $i = 1, 2$ and $d = \log(k_2/k_1)$.

(ii) The Rényi distance of order β :

$$d_R^\beta(\theta_1, \theta_2) = \frac{1}{\beta - 1} \left[\log \left(h_1 \int_0^\infty x^{g_1} (b_1 + L_1 x)^{e_1} (b_2 + L_2 x)^{e_2} dx \right) + \log \left(h_2 \int_0^\infty x^{g_2} (b_1 + L_1 x)^{m_1} (b_2 + L_2 x)^{m_2} dx \right) \right],$$

where $h_1 = k_2^\beta k_1^{1-\beta}$, $h_2 = k_1^\beta k_2^{1-\beta}$, $g_1 = (L_1 - 1)(1 - \beta) + (L_2 - 1)\beta$, $g_2 = (L_1 - 1)\beta + (L_2 - 1)(1 - \beta)$, $e_1 = (\alpha_1 - L_1)(1 - \beta)$, $e_2 = (\alpha_2 - L_2)\beta$, $m_1 = (\alpha_1 - L_1)\beta$ and $m_2 = (\alpha_2 - L_2)(1 - \beta)$, and $0 < \beta < 1$.

(iii) The Hellinger distance: $d_H(\theta_1, \theta_2) = 2 \left(1 - \sqrt{k_1 k_2} \int_0^\infty x^{(a_1+a_2)/2} (b_1 + L_1 x)^{f_1} (b_2 + L_2 x)^{f_2} dx \right)$, where $f_i = \frac{\alpha_i - L_i}{2}$, for $i = 1, 2$.

(iv) The Bhattacharyya distance: $d_B(\theta_1, \theta_2) = -\log \left(\sqrt{k_1 k_2} \int_0^\infty x^{(a_1+a_2)/2} (b_1 + L_1 x)^{f_1} (b_2 + L_2 x)^{f_2} dx \right)$.

Fig. 5. Explicit distances under the \mathcal{G}^0 model.

in *Advances in Imaging and Electron Physics*, P. W. Hawkes, Ed. Academic, 1995, no. 91, pp. 37–135.

- [41] —, “Bounds on triangular discrimination, harmonic mean and symmetric chi-square divergences,” *Journal of Concrete and Applicable Mathematics*, vol. 4, pp. 91–111, 2006.
- [42] J. Burbea and C. Rao, “Entropy differential metric, distance and divergence measures in probability spaces: a unified approach,” *Journal of Multivariate Analysis*, vol. 12, pp. 575–596, 1982.
- [43] S. Aviyente, “Divergence measures for time-frequency distributions,” in *Seventh International Symposium on Signal Processing and Its Applications (SISSPA)*, vol. 1, July 2003, pp. 121–124.
- [44] A. K. Seghouane and S. I. Amari, “The AIC criterion and symmetrizing the Kullback-Leibler divergence,” *IEEE Transactions on Neural Networks*, vol. 18, no. 1, pp. 97–106, 2007.
- [45] R. Piessens, E. de Doncker-Kapenga, C. W. Uberhuber, and D. K. Kahaner, *QUADPACK: A Subroutine Package for Automatic Integration*. New York: Springer-Verlag, 1983.
- [46] D. Blatt and A. O. Hero, “On tests for global maximum of the log-

likelihood function,” *IEEE Transactions on Information Theory*, vol. 53, pp. 2510–2525, July 2007.

- [47] Wolfram Research, Inc., *Mathematica*, Champaign, Illinois, 2005, version 5.2.



Abraão D. C. Nascimento holds B.Sc. and M.Sc. degrees in Statistics from the Universidade Federal de Pernambuco (UFPE), Brazil, and he is currently a doctorate student in Statistics at the same University. His research interests are stochastic models and distances.

$$\int_0^\infty \frac{x^a}{(b+nx)^c} dx = \frac{b^{-c} \left(\frac{n}{b}\right)^{-1-a} \Gamma(1+a) \Gamma(-1-a+c)}{\Gamma(c)},$$

$$\int_0^\infty \frac{\log(b+nx)x^a}{(b+nx)^c} dx = \frac{1}{\Gamma(c)} \left(b^{-c} \left(\frac{n}{b}\right)^{-1-a} \Gamma(1+a) \Gamma(-1-a+c) (\log(b) + \psi^{(0)}(c) - \psi^{(0)}(-1-a-c)) \right),$$

$$\int_0^\infty \frac{\log(b_1+n_1x)x^a}{(b_2+n_2x)^c} dx = \frac{b_1 b_2^{-c} \pi \csc(a\pi)}{n_1} \left(\frac{n_2^2 (b_1/n_1)^{2-a} c {}_2F_1\left(2+a, 1+c; 3+a; \frac{b_1 n_2}{b_2 n_1}\right)}{b_2^2} - \frac{2+a}{2+3a+a^2} \left(\frac{b_2 n_1 - b_1 n_2}{b_2 n_1}\right)^{-c} + \frac{(n_2/b_2)^{-a} \Gamma(-1-a+c) {}_3F_2\left(1, 1, -a+c; 2, 1-a; \frac{b_1 n_2}{b_2 n_1}\right)}{\Gamma(1-a) \Gamma(c)} + \frac{n_1 (b_2/n_2)^{1+a} \Gamma(-1-a+c)}{b_1 \Gamma(-a) \Gamma(c)} \left(\log\left(\frac{n_2}{n_1 b_2}\right) + \psi^{(0)}(-1-a+c) - \psi^{(0)}(-a) + \pi \cot(a\pi) \right) \right),$$

where ${}_2F_1(\cdot, \cdot; \cdot; \cdot)$ and ${}_3F_2(\cdot, \cdot, \cdot; \cdot, \cdot; \cdot)$ are hypergeometric functions,

$$\int_0^\infty \frac{\log(x)x^a}{(b+nx)^c} dx = -\frac{1}{\Gamma(c)} \left[b^{-c} (n/b)^{-1-a} \Gamma(1+a) \Gamma(-1-a+c) (-H_{\lfloor a+1 \rfloor} + H_{\lfloor -1-a+c \rfloor} + \log(n/b)) \right],$$

where H_n is the n th harmonic number, and

$$\int_0^\infty x^a (b_1+n_1x)^{c_1} (b_2+n_2x)^{c_2} dx = b_1^{c_1} b_2^{c_2} \pi \csc((c_2+a)\pi) \left[-\frac{\left(\frac{n_1}{b_1}\right)^{-1-c_2-a} \left(\frac{n_2}{b_2}\right)^{c_2} \Gamma(-1-c_1-c_2-a) {}_2F_1\left(-c_2, -1-c_1-c_2-a; -c_2-a; \frac{b_2 n_1}{b_1 n_2}\right)}{\Gamma(-c_1) \Gamma(-c_2-a)} + \frac{\left(\frac{n_2}{b_2}\right)^{-1-a} \Gamma(1+a) {}_2F_1\left(-c_1, 1+a; 2+c_2+a; \frac{b_2 n_1}{b_1 n_2}\right)}{\Gamma(-c_2) \Gamma(2+c_2+a)} \right].$$

Fig. 6. Integral identities under the \mathcal{G}^0 model.



Renato J. Cintra earned both his B.Sc. and M.Sc. degrees in Electrical Engineering from UFPE, Brazil, in 1999 and 2001, respectively. After a professional experience in petroleum industry, he started doctorate studies in Electrical Engineering. In 2003 he spent one academic year at the University of Calgary as a visiting graduate student, addressing Biomedical Engineering problems. In 2005, he completed his doctorate and joined the Department of Statistics at UFPE. His long term topics of research include theory and methods for digital signal

processing, communications systems, and applied mathematics. He performs routinely reviewing work for major peer-review journals. Since 2008, he is working at the University of Calgary, Canada, as a visiting research fellow.



Alejandro C. Frery graduated in Electronic and Electric Engineering from the Universidad de Mendoza, Argentina. His M.Sc. degree was in Applied Mathematics (Statistics) from the Instituto de Matemática Pura e Aplicada (Rio de Janeiro) and his Ph.D. degree was in Applied Computing from the Instituto Nacional de Pesquisas Espaciais (São José dos Campos, Brazil). He is currently with the Instituto de Computação, Universidade Federal de Alagoas, Maceió, Brazil. His research interests are statistical computing and stochastic modelling.